UNIVERSITAT DE BARCELONA

Spin crossover supramolecular coordination compounds: design, synthesis and properties

Mohanad D .Darawsheh

Contents

CHAPTER 2: Design of Host-Guest Triple-Stranded Helicates

2.1 Introduction

The preparation of polynuclear compounds containing paramagnetic centers is still subject of interest from the fundamental and that of applications point of view. The design of new ligands is the first step in the synthetic inorganic chemistry process that leads to the desired polynuclear metal topology and metallo-supramolecular systems. Our group has been involved in the last years in designing of novel β-diketone ligands and using them in the preparation of magnetic coordination clusters[1–6] with promising applications such as quantum computing.[7–9]

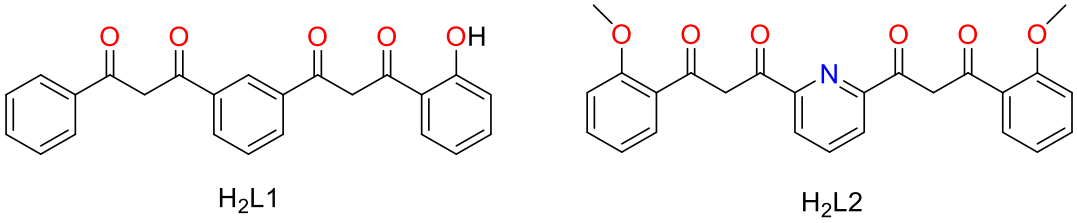

Figure 2.1: Left) 1-(2-hydroxyphenyl)-3-(3-(3-oxo-3-phenylpropanoyl)phenyl)propane-1,3-dione (H_2L1) Right) 1,3-*bis*-(3-oxo-3-(2-methoxyphenyl)-propionyl)-pyridine (H_2L2).

In general, these ligands contain multifunctional pockets consisting mainly of poly-β-diketone, phenolyl or dipicolinate groups. For example, the ligand H_2L1 was prepared in collaboration with organic chemistry group at the University of Barcelona (see appendix I). The ligand contains two β-diketone pockets separated by a phenyl spacer. The most interesting aspect of this ligand is its asymmetric character, with the terminal sides consisting of phenyl and phenolyl groups, respectively. This asymmetry makes this ligand a promising platform for preparing metal clusters for quantum computing, featuring inequivalence of coordination environments around the spin carriers.[2,7] In addition, H_2L1 contains two different ionisable protons with different acidity, the phenol and the β-diketone groups. This can allow for the preparation of supramolecular assemblies like dinuclear triple-stranded helicates using a suitable transition metal keeping the phenol group protonated.

Indeed, the neutral dinuclear helicate $Fe_2(H_2L1)_3$ (**i**) was prepared by the reaction of $FeCl_3$ with H_2L1 in CH_2Cl_2 in the molar ratio 2:3. The structure consists of three ligands

wrapping around two Fe(III) ions to form a dinuclear triple stranded helicate (Figure 2.2) [see appendix I for detailed crystallographic data and structural parameters]. The pseudo-octahedral geometry around each metal is provided by chelation with three β-diketone moieties. In each discrete helicate within the lattice, the two metal ions have the same chirality. Thus each complex is either *ΔΔ* (*P*) or *ΛΛ* (*M*) leading to a racemic mixture of both enantiomers in the crystal. This helical configuration is possible thanks to the torsion around the C-C bonds connecting the central phenyl group with the *β*-diketone moieties, which show an average value of 30.40° through the helicate. The OH groups are mainly involved in intramolecular hydrogen bonds with the closest lying coordinated oxygen of the β-diketone. The Fe···Fe intra-helical distance is 7.179 Å and the helical cavity encloses a solvent accessible volume of 19.4 $Å^3$ as calculated using Olex2 1.2[10] without the presence of any encapsulated species (e.g. solvent molecules).

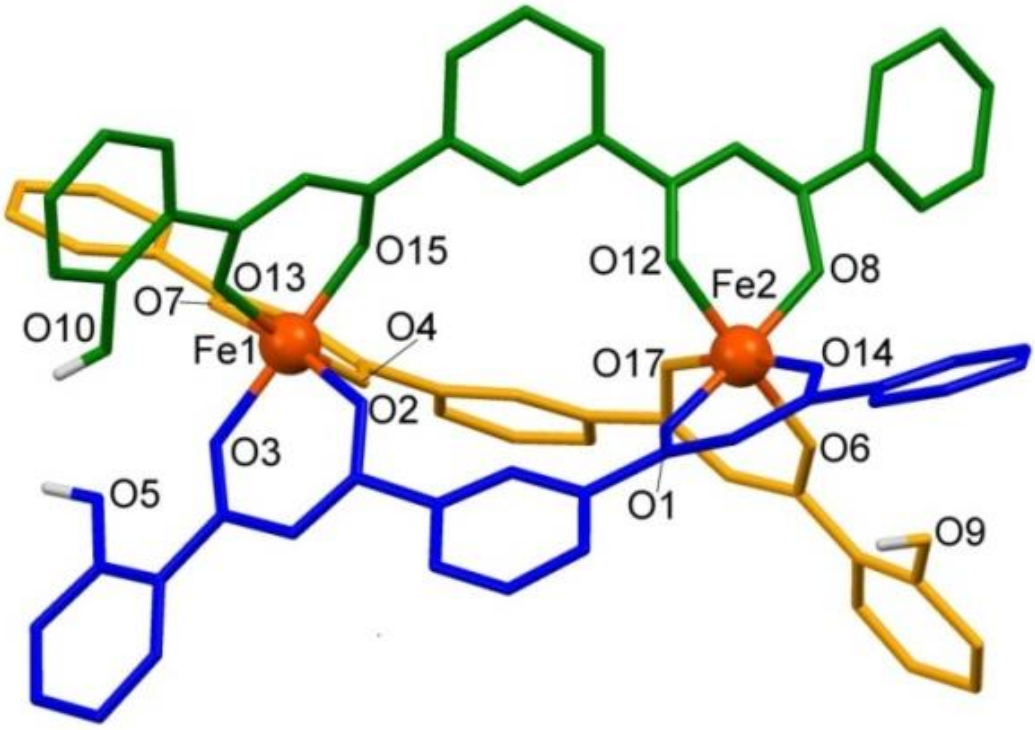

Figure 2.2: Molecular representation of $[Fe_2(H_2L1)_3]$ in compound (**i**) showing helical structure around the metals. Only the hydrogen atoms on the oxygen atoms are shown. Only metals and heteroatoms are labeled. The three ligands are shown in different colors.

Another example of such *β*-diketone ligands is H_2L2 (Figure 2.1), where the presence of the central dipicolinate moiety allows for the encapsulation of specific species *via* coor-

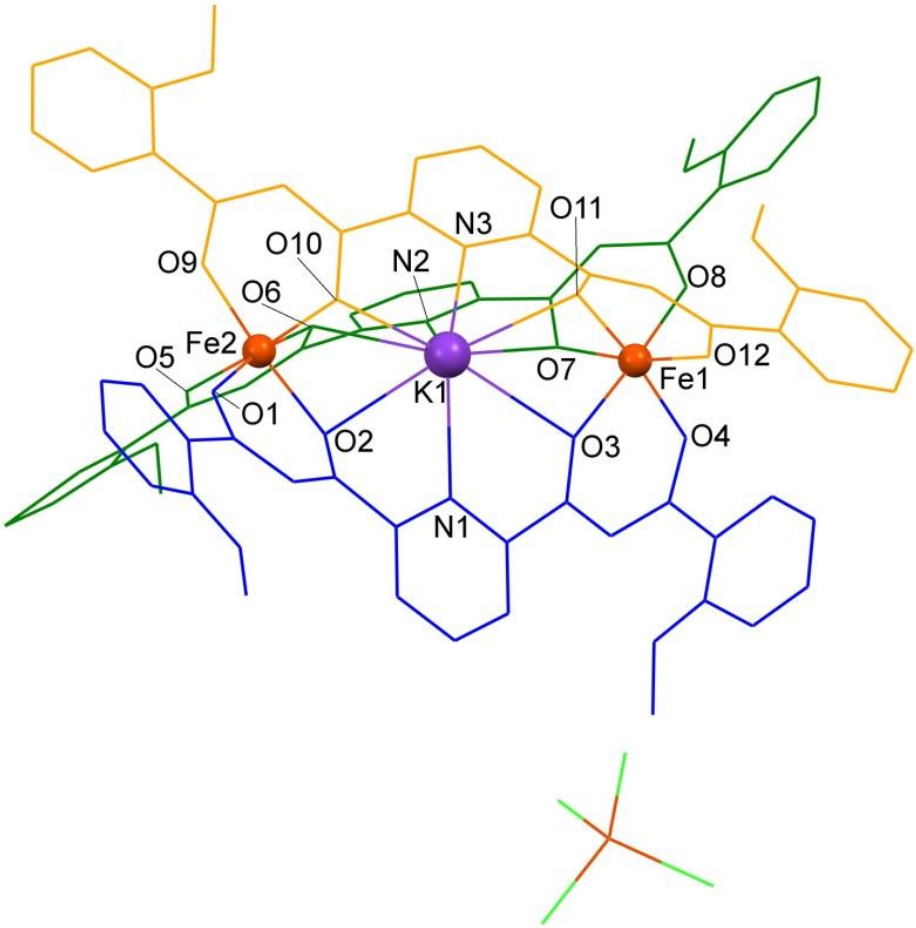

Figure 2.3: Molecular representation of [K⊂Fe_2 (H_2L2)$_3$]($FeCl_4$) in compound (**ii**). Only metals and heteroatoms involved in coordination bond are labeled. The three ligands are shown in different colors in wireframe style.

dination bonds. The ligand was used to prepare the compound [K⊂Fe_2(H_2L2)$_3$]($FeCl_4$) by the reaction of $FeCl_3 \cdot 3H_2O$ with H_2L2 in THF with the presence of K_2CO_3 as base. The structure in this compound (**ii**), formed by coordination of the β-diketone groups around the two Fe(III) centers is similar to this seen in compound **i**. However, a K^+ is encapsulated inside the cavity forming nine coordination bonds with three dipicolinate groups (Figure 2.3, see appendix I for detailed crystallographic data and structural parameters) yielding a mesocate in contrast to the helical structure seen in compound (**i**). The volume of the cavity is suitable for such encapsulation since the K^+ ion with a volume of ca. 15.60 $Å^3$ (K^+ radius[11] 1.55 Å) can fit perfectly in the cavity, which has a volume of 34.6 $Å^3$ (calculated using olex2 1.2[10]). The methoxy groups are in *trans* conformation with respect to the *β*-diketone groups, which is probably favored by the

C-H···O hydrogen bond with the C-H of the *β*-diketone moiety. It's worth to mention, that this compound shows a promising DNA binding activity thanks to its helical structure and its positive charge, which facilitates the interaction with the phosphate group of the DNA with negative charge.

The versatility of the synthetic approach to produce poly-*β*-diketone arises from the ability of use different spacers and terminal groups, which affords the possibility of prepare a large variety of novel helical systems. The disadvantage of these groups is the that presence of oxygen donors facilitates the oxidation of some divalent transition metal ions [i.e. Fe(II)] to the trivalent ones. However, suitable *β*-diketone containing ligands can be used as precursor for preparing pyrazolyl-pyridine containing ligands, which lead to nitrogen-coordinated complexes. This approach was used to prepare polypyrazolyl ligands [Derivatives of 2,6-bis(pyrazol-3-yl)pyridine (3-bpp)] which exhibit novel SCO behavior thanks to the suitable crystal field and the large number of supramolecular interactions provided by the ligands.[12–18] This approach can be used to prepare bis-pyrazolylpyridine ligands suitable for the formation of helicates. The pyrazolylpyridine moiety provides a suitable environment around the transition metal ion to exhibit spin crossover [*i.e.* Fe(II)] and stabilizes the low oxidation number of such metals in contrast to the *β*-diketone moiety. Moreover, the H-N group of the pyrazole ring can play a powerful role of encapsulation of hydrogen acceptor ions inside the helical cavity.

2.2 Anion-Encapulated Triple-Stranded Helicates Using Bis-pyrazolylpyridine Ligands

As mentioned above, poly-β-diketone ligands are suitable candidates to prepare triple-stranded helicates. The presence of oxygen atoms facilitates the oxidation of divalent transition metal ions [*i.e.* Fe(II)] while the acidity of the *β*-diketone protons yields stable neutral dinuclear triple-stranded helicates via deprotonation which makes the encapsulation of ionic species more difficult. However, *β*-diketone ligands serve as precursors for the preparation of pyrazolylpyridine containing ligands via a simple ring closure reaction. In this chapter we will present two bis-pyrazolylpyridine ligands prepared from poly-*β*-diketone precursors and their use for the preparation of novel triple-stranded helicates with encapsulated anions.

Ligand H_2L3 is a poly-β-diketone ligand which has two pyridine rings at both ends. The synthesis of this ligand is achieved using the well-known Claisen condensation of 1,3-diacetylbenzene and 2-ethylpicolinate, as previously performed for similar poly-β-diketone ligands synthesized in our group[4,5] (Figure 2.4). H_2L3 serves as precursor for the preparation of bis-pyrazolylpyridine, H_2L4, *via* the ring closure reaction with hydrazine[19] (Figure 2.5). The reactants were refluxed in methanol to produce H_2L4 as a white solid after 20 h in around 50% yield.

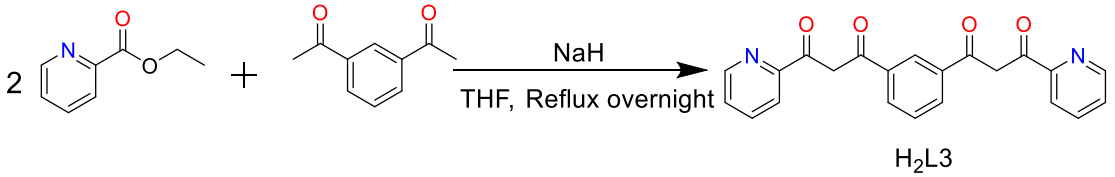

Figure 2.4: Synthesis of 1,3-bis-(1-oxo-3-(pyridine-2-yl)-propionyl)-benzene, H_2L3.

The Ligand H_2L4 has three main features: bis-pyrazolylpyridine chelating sites, a relatively rigid spacer with the ability of twisting and additional hydrogen donor NH groups. All those simple parts can be combined to facilitate the formation of supramolecular triple-stranded helicates with first raw transition metals. Three pyrazolylpyridine groups afford the chelating sites suitable for octahedral geometry around the metal ions. Moreover, this N_6 coordination sphere is a suitable environment of crystal field around the metals ions (*i.e.* Fe^{2+}) to exhibit spin crossover behavior.[20,21]

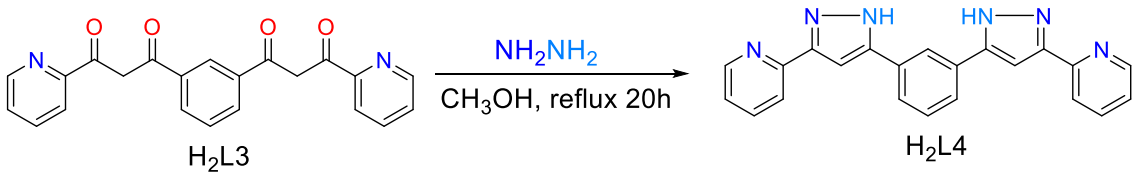

Figure 2.5: synthesis of 1,3-bis-(1-(pyridine-2-yl)-pyrazol-3-yl)-benzene, H_2L4.

The ditopic nature of this ligand arising from two chelating sites linked by a rigid aromatic spacer, gives the possibility to link two metal ions and yield stable dinuclear helicates. Large and more flexible spacers like aliphatic chains are more likely form polynuclear cages and polymers.[22] However, H_2L4 can twist around the C-C bonds linking the aromatic rings and give the suitable geometry (i.e. octahedral) and symmetry (*i.e.* 3 fold symmetry) around two metal centers. Importantly, the additional NH group can play a major role in the assembly of supramolecular structures by hosting, through encapsulation, small anions with hydrogen acceptor ability. Indeed, Cl-encapsulated

$[Co(II)_2]$ and $[Ni(II)_2]$ triple-stranded helicates were synthesized where Cl^- is encapsulated inside the cavity (see below). The same approach was used for the synthesis of $[Fe(II)_2]$ helicates exhibiting SCO, which could be tuned by changing the guest species (Chapter 3).

2.3 $[Co(II)_2]$ and $[Ni(II)_2]$ Triple-Stranded Helicates Using H_2L4

2.3.1 Synthesis and Crystal Structure of $Cl\subset[Co_2(H_2L4)_3]Cl(PF_6)_2\cdot4CH_3OH\cdot0.25C_4H_{10}O$ (iii) and $Cl\subset[Ni_2(H_2L4)_3]Cl(PF_6)\cdot2.5CH_3OH$ (iv)

Complexes (**iii)** and (**iv**) were prepared from the reaction of $CoCl_2\cdot6H_2O$ or $NiCl_2$ salts, respectively, with H_2L4 (3:2 stoichiometry) in CH_3OH at room temperature. The resulting solutions were treated with two equivalent of NBu_4PF_6 and orange single crystals were isolated in both cases by slow diffusion of diethyl ether into the methanolic solution after a few days.

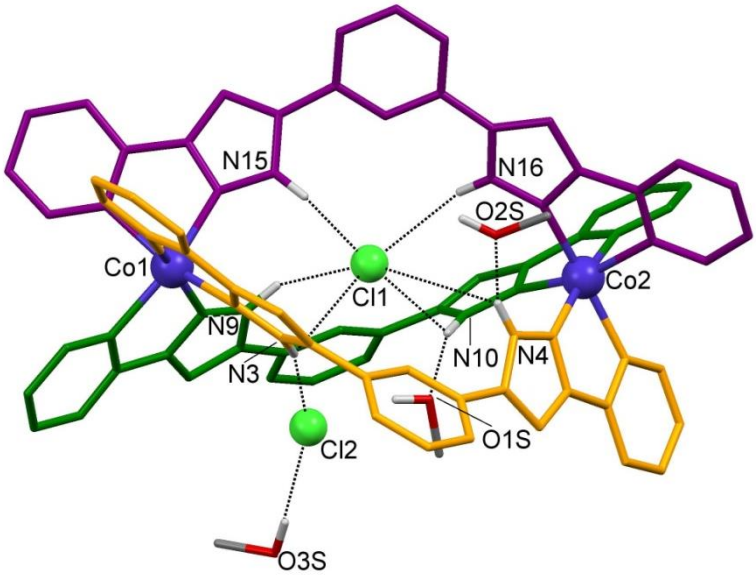

Figure 2.6: Molecular representation of $\{Cl\subset[Co_2(H_2L4)_3]Cl\}^{2+}$ cation in **iii** showing the hydrogen bonding between the NH groups and the two Cl^- counterions and the MeOH molecules. PF_6^- ions and one MeOH molecules and partial ether are omitted for clarity. Only the hydrogen atoms on the pyrazole nitrogen atoms are shown. Only metals and heteroatoms involved in hydrogen bonding are labeled.

Both compounds crystallize in the tetragonal non-centrosymmetric space group $I4_1cd$ (Z=16). Crystal data and selected structural parameters at 100 K are shown in Tables 2.1-2.3. The asymmetric units consist of a cationic $\{Cl\subset[Co_2(H_2L4)_3]\}^{3+}$ or $\{Cl\subset[Ni_2(H_2L4)_3]\}^{3+}$ helicates, one Cl^- and two PF_6^- counterions, four and five MeOH molecules, respectively, and in the case of **iii** half ether molecule with 0.25 partial occupancy. One PF_6^- ion exhibits disorder over two positions in both compounds.

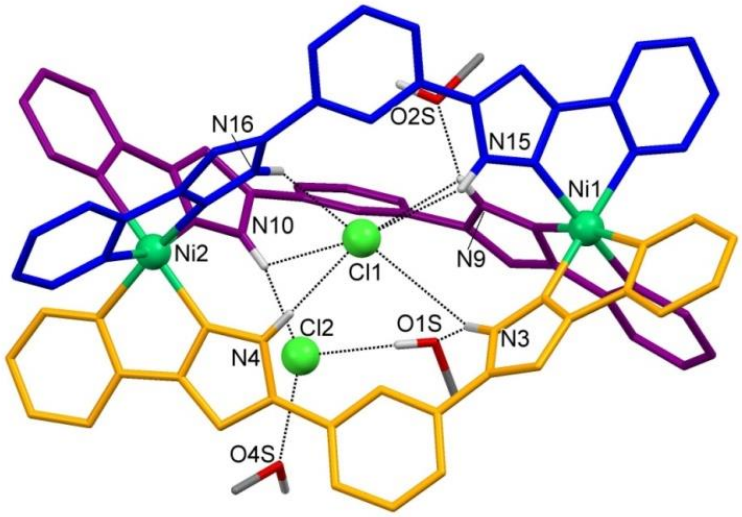

Figure 2.7: Molecular representation of $\{Cl\subset[Ni_2(H_2L4)_3]Cl\}^{2+}$ cation in **iv** showing the hydrogen bonding between the NH groups and the two Cl^- counterions and the MeOH molecules. PF_6^- ions and two MeOH molecules are omitted for clarity. Only the hydrogen atoms on the pyrazole nitrogen atoms are shown. Only metals and heteroatoms involved in hydrogen bonding are labeled.

Both metal ions in each helicate have the same chirality. Each complex is thus either $\Delta\Delta$(*P*) or $\Lambda\Lambda$(*M*), leading to a racemic mixture of the two enantiomers within the lattice. The intra-helical Co1···Co2 and Ni1···Ni2 distances are 9.771 Å and 9.791 Å, respectively. The helicate encloses a cavity of volume of 26.5 and 37.8 $Å^3$ for **iii** and **iv**, respectively, as calculated using Olex2 2.1[10] making it suitable for hosting small anions. Indeed, the helical cavity contains one chloride ion Cl1 that participates in six hydrogen bonds, interacting with the N-H groups of the pyrazolyl moieties. Two of these hydrogen bonds in one side of the helicate are much stronger than the others [N10-H···Cl1 = 2.381 and N16-H···Cl1 = 2.249 Å] and [N4-H···Cl1 = 2.517 and N16-H···Cl1 = 2.497 Å] for **iii** and **iv**, respectively. As a result, the Cl^- ion is located closer to one metal than to the other [Co1···Cl1 = 4.710Å, Co2···Cl1 = 5.070Å, Ni1···Cl1 =

5.093 and Ni2···Cl1 = 4.705Å]. The second chloride ion, Cl2, is located out of the cavity and it is participating in a strong hydrogen bond with one NH group [N3-H···Cl2 = 2.249Å or N10-H···Cl2 = 2.251 Å] (Figure 2.6). The methanol molecules also form strong hydrogen bonds with the N-H groups which closer to one of the metal ions. One of these solvent molecules is also involved in a hydrogen bond with the outer chloride ion.

The $(M\text{-}N)_{avg}$ distances are typical for HS state in both complexes [$(Co\text{-}N)_{avg}$ = 2.139.and $(Ni\text{-}N)_{avg}$ = 2.100]. The difference in cation-anion interactions does not yield here in any case the distinct spin behavior observed in Fe(II) complexes (chapter 3). The packing with in the lattice consists of helicates organized in sheets connected together with $\pi-\pi$ and C-H… π interactions of the aromatic rings. Every helicate is surrounded by five close neighbors. These sheets are separated by hydrophilic layers containing the counter ions and the solvent molecules (the packing is similar to the one seen for compound **1**, and is discussed in detail in Chapter 3).

Table 2.1: Crystallographic data for **iii** and **iv**.

Compound	**iii**	**iv**
Formula	C_{66} H_{48} N_{18} Co_2, 2(PF_6),4(C H_4 O), 0.25(C_4 H_{10} O), 2(Cl)	C_{66} H_{48} N_{18} Ni_2, 2(PF_6), 5(C H_4 O), 2(Cl)
M_r	1720.13	1731.69
Wavelength	0.7749	0.71073
T (K)	100	100
Crystal system	Tetragonal	Tetragonal
Space group	$I4_1cd$	$I4_1cd$
Z	16	16
a=*b* [Å]	24.4100(8)	24.532(3)
c [Å]	52.846(2)	52.701(7)
$\alpha = \beta = \gamma$ [º]	90	90
V [Å^3]	31488(2)	31716(9)
ρ_{calc} (gcm^{-3})	1.451	1.447
μ(mm^{-1})	0.764	0.671
Independent reflections	13907	8534
Restraints/parameters	159/1022	187/1021
Goodness of fit on F^2	1.031	1.038
Final R_1/wR_2 [$I>2\sigma(I)$]	0.0555/0.1569	0.0731/0.1902
Final R_1/wR_2 [all data]	0.0607/0.1636	0.1041/0.2147
Largest diff. peak and hole (eÅ^3)	1.622/-0.599	0.914/-0.677

Table 2.2: Selected interatomic distances [Å] found in **iii**.

Co1-N1	2.213(7)	Co1-N2	2.105(5)
Co1-N7	2.141(5)	Co1-N8	2.100(7)
Co1-N13	2.203(5)	Co1-N14	2.099(7)
Co2-N5	2.104(5)	Co2-N6	2.173(6)
Co2-N11	2.099(5)	Co2-N12	2.179(5)
Co2-N17	2.118(7)	Co2-N18	2.129(5)
Co1⋯Co2	9.771(1)	Co1⋯Cl1	4.710(2)
Co2⋯Cl1	5.070(2)	N3-H⋯Cl1	3.156
N4-H⋯Cl1	3.465	N9-H⋯Cl1	2.490
N10-H⋯Cl1	2.381	N15-H⋯Cl1	2.734
N16-H⋯Cl1	2.249	N3-H⋯Cl2	2.249
N4-H⋯O1S	1.969	N10-H⋯O2S	1.879
O3S-H⋯Cl2	2.260		

Table 2.3: Selected interatomic distances [Å] found in **iv**.

Ni1-N1	2.13(1)	Ni1-N2	2.07(1)
Ni1-N7	2.11(2)	Ni1-N8	2.07(1)
Ni1-N13	2.09(1)	Ni1-N14	2.09(2)
Ni2-N5	2.08(2)	Ni2-N6	2.10(1)
Ni2-N11	2.08(1)	Ni2-N12	2.18(2)
Ni2-N17	2.05(1)	Ni2-N18	2.14(1)
Ni1⋯Ni2	9.791(3)	Ni1⋯Cl1	5.093(5)
Ni2⋯Cl1	4.705(5)	N3-H⋯Cl1	3.144
N4-H⋯Cl1	2.517	N9-H⋯Cl1	3.398
N10-H⋯Cl1	3.139	N15-H⋯Cl1	2.840
N16-H⋯Cl1	2.497	N10-H⋯Cl2	2.251
N3-H⋯O1S	1.887	N9-H⋯O2S	1.920
N15-H⋯O5S	2.575	O3S-H⋯Cl2	2.998

2.3.2 Magnetic Properties of the Cl⊂Co_2 (iii) and Cl⊂Ni_2 (iv) Helicates

Magnetic susceptibility measurements of compound **iii** and **iv** were carried out on polycrystalline samples in the temperature range 2-300 K and 2-320 K, respectively. To avoid possible orientation effects, the measurements for **iii** were performed under a constant magnetic field of 0.01 T (below 100 K) or 0.5 T (above 80 K). For **iv**, the measurements were done under constant magnetic field of 0.5 T. The plots of $\chi_m T$ vs. T are shown in Figure 2.8.

For **iii**, the $\chi_m T$ value at 300 K (5.70 $cm^3mol^{-1}K$) exceeds the spin-only value of two non-interacting Co(II) (two S = 3/2 centers, spin-only value of 3.75 $cm^3mol^{-1}K$ for g =

2). However, the value is close to the one expected when the spin momentum and orbital momentum exist independently. {6.76 $cm^3mol^{-1}K$; χ_mT = 1/8[L(L+1)+4S(S+1)]}. This behavior arises from the spin-orbit coupling (*i.e.* contribution of the orbital momentum of the $^4T_{1g}$ ground state) displayed by high-spin Co(II) in octahedral surrounding.

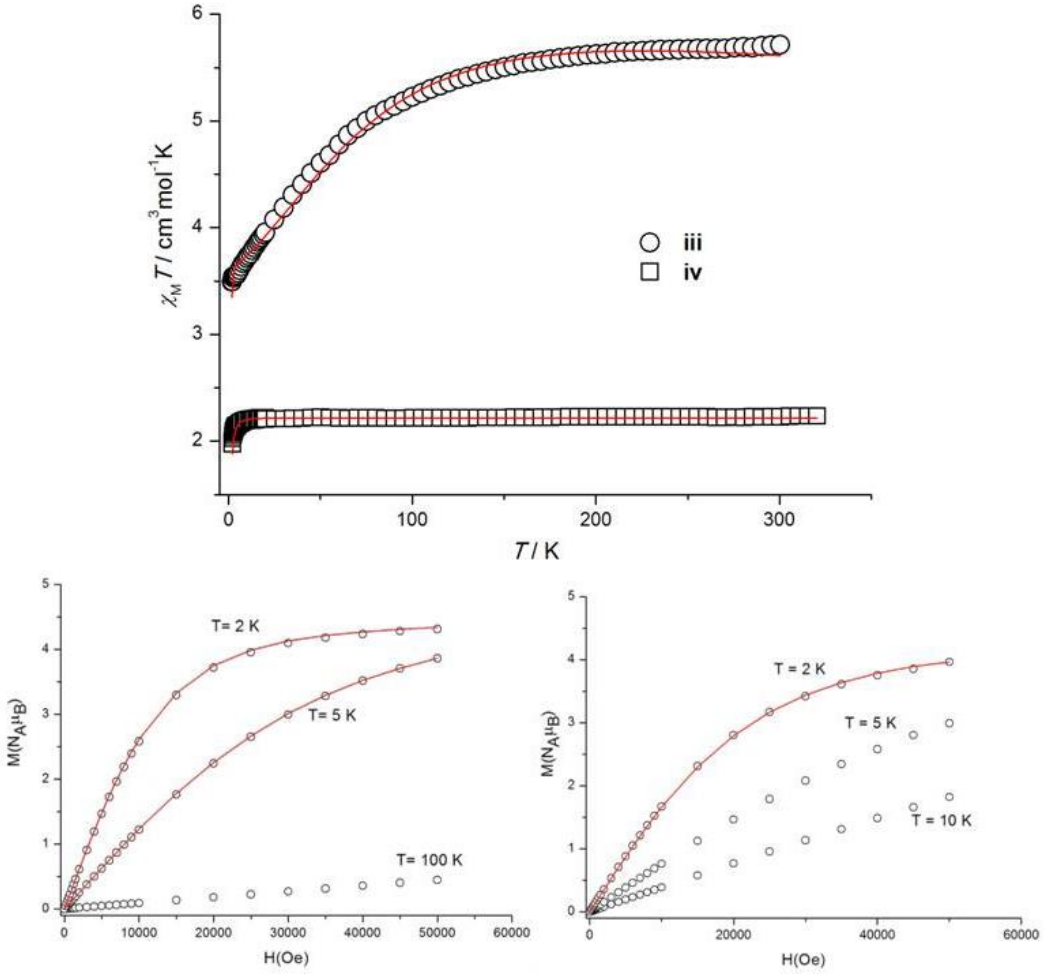

Figure 2.8: Top: Temperature dependence of χ_mT in **iii** and **iv**. Bottom: Field dependence of the magnetization in **iii** (left) and **iv** (right). Red line is the best fit using PHI program yielding $\alpha = 1.096$, $\lambda = -151.9$ cm^{-1}, $\Delta = -323.4$ cm^{-1}, $\delta = -7.8$ cm^{-1} and $zJ = 0.0209$ $cm^{-1}$for **iii** and g = 2.11, D = -2.44 cm^{-1} and E = 0.022 for **iv** (see text for details).

Below 200 K, χ_mT value decreases to reach a value of 3.50 $cm^3mol^{-1}K$ at 2 K. This behavior can be attributed to the typical magnetic anisotropy of Co(II) rather than to antiferromagnetic exchange interactions between the two centers in the helical structure (Co···Co distance is 9.771Å). This is supported by the field dependence of the magnetization measured at 2 K which reaches saturation of value 4.2 μ_B (Figure 2.8).

This value corresponds to 2.1 μ_B per Co(II) ion which is smaller than the expected value of 3 μ_B expected for $S = 3/2$. It agrees however, with the one derived from the model of Co(II) complexes which consider only the population of the Kramer doublet (below 30 K) and thus an effective spin $S_{eff} = ½$ is assumed for this low-lying doublet ($\chi_m T$ in the range 1.5-1.7 $cm^3mol^{-1}K$ and saturation magnetization of 2.2 μ_B per Co(II) ion).[23] *AC* magnetic susceptibility measurements in zero-field were also performed and indicate no sign of any zero-field out-of-phase *ac* susceptibility signal down to 1.9 K.

The analysis of the magnetic properties of six-coordinated HS Co(II) complexes is more complicated than spin-only systems as a result of the strong orbital contribution of the ground orbital triplet $^4T_1$ to the magnetic moment.[24] The distortion from the octahedral coordination sphere and the spin-orbit coupling remove the degeneracy of the ground and the excited states, leading to an energy spectrum where the two-lying levels correspond to $Ms = \pm 1/2$ and $Ms = \pm 3/2$ states.

The magnetic susceptibility data was analyzed using the following Hamiltonian[23,25,26] considering two isolated Co(II) ions within the helicate

$$\hat{H} = -\alpha\lambda\hat{L}\hat{S} + \Delta\left[\hat{L}_z^2 - \hat{L}(\hat{L}+1)/3\right] + \delta\left(\hat{L}_x^2 - \hat{L}_y^2\right) + \beta H(-\alpha\hat{L} + g_e\hat{S})$$

Where Δ and δ are the axial and rhombic energy gap between the states split by distortion of the coordination sphere, λ is the spin-orbit coupling factor, α is the orbital reduction factor. The other symbols have their usual meanings. The terms of this Hamiltonian account for spin-orbit coupling, crystal field splitting and Zeeman interaction, respectively. With introducing the intermolecular interaction parameter *zJ*, the best fit using PHI program gives λ = -151.9 cm^{-1}, α = 1.096, Δ = -323.4 cm^{-1}, and zJ = 0.0209 cm^{-1} (Figure 2.8). These values are similar to these observed for distorted octahedral Co (II) complexes.[23,25–33] The reduction of the λ from that of free Co (II) (λ_0 = 172 cm^{-1}) is reasonable taking into account the moderate crystal field splitting (Δ = -323.4 cm^{-1}). The α value falls in the expected range of 1.0-1.5 and Δ for high spin Co(II) is usually found in the range 200-800 cm^{-1}.[23,28] The results indicate only very weak intermolecular interaction in agreement with the large Co···Co intermolecular distance (8.826 Å) seen in the crystal structure.

The Δ value indicates a low to moderate distortion from the octahedral geometry around Co(II) ions. The distortion from the ideal octahedron can be described using the Σ factor

(angular distortion)[34] and continuous symmetry measures[35] (interatomic distances distortion). The average values for the Co(II) ions in the helical structure equal 94.03°, 2.277 and 9.235 for Σ, *S(Oh)* and *S(itp)*, respectively. The latter values indicate moderate distortion from octahedral toward trigonal prism where the geometry is still close to octahedral. This is in agreement with the crystal field splitting parameters. Finally, simulation of the field dependence of the magnetization data using the above Hamiltonian and the factors deduced from fitting of the magnetic susceptibility reproduces very well the experimental data (Figure 2.8).

For compound **iv**, the $\chi_m T$ curve remains constant in the range 320-10 K, with a value of 2.22 $cm^3mol^{-1}K$, which is typical for two well isolated Ni(II) ions with *g* slightly higher than 2. The decrease in the value below 10 K is mostly due to zero-field splitting arising from the distortion in the coordination sphere around Ni(II) ions. The interaction between the Ni(II) ions is not expected since the Ni···Ni distance is 9.791 Å. The molar magnetic susceptibility data and the magnetization data at 2 K were fitted using PHI program[36] according to the following Hamiltonian:

$$\hat{H} = D\left(\hat{S}_z{}^2 - \frac{1}{3}\hat{S}^2\right) + E\left(\hat{S}_x{}^2 - \hat{S}_y{}^2\right) + \mu_B \hat{S} g B$$

Where *D* and *E* stand for axial and rhombic ZFS parameters, respectively, $\hat{S}$ is total spin operator and $\hat{S}_i$ (*i*= *x,y, z*) are operators of its components, *B* is magnetic induction and μ_B is Bohr magneton. The best fit for both data sets gave an average value of g = 2.11, D = -2.44 cm^{-1} and E= 0.022 cm^{-1}.This is agree with what observed in other Ni(II) complexes.[37]

2.3.1 Mass Spectrometry of the Cl⊂Co_2 (iii) and Cl⊂Ni_2 (iv) Helicates

Mass spectrometry for compounds **iii** and **iv** were measured in CH_3CN using the positive ion electrospray (ESI^+) technique.

In compound **iii**, the most prominent peaks were ascribed to the free ligand. However, a low intensity peak corresponding to the dinuclear triple-stranded helicate $[Co_2(HL4)_3]^{2+}$ was observed at m/z = 603.63 (Figure 2.9). In this ion, three N-H units have been deprotonated and one cobalt ion has +3 charge. The isotopic distribution of this peak is consistent with the theoretical one as shown in Figure 2.9. No peaks corresponding to the Cl^- encapsulated triple stranded helicate were observed.

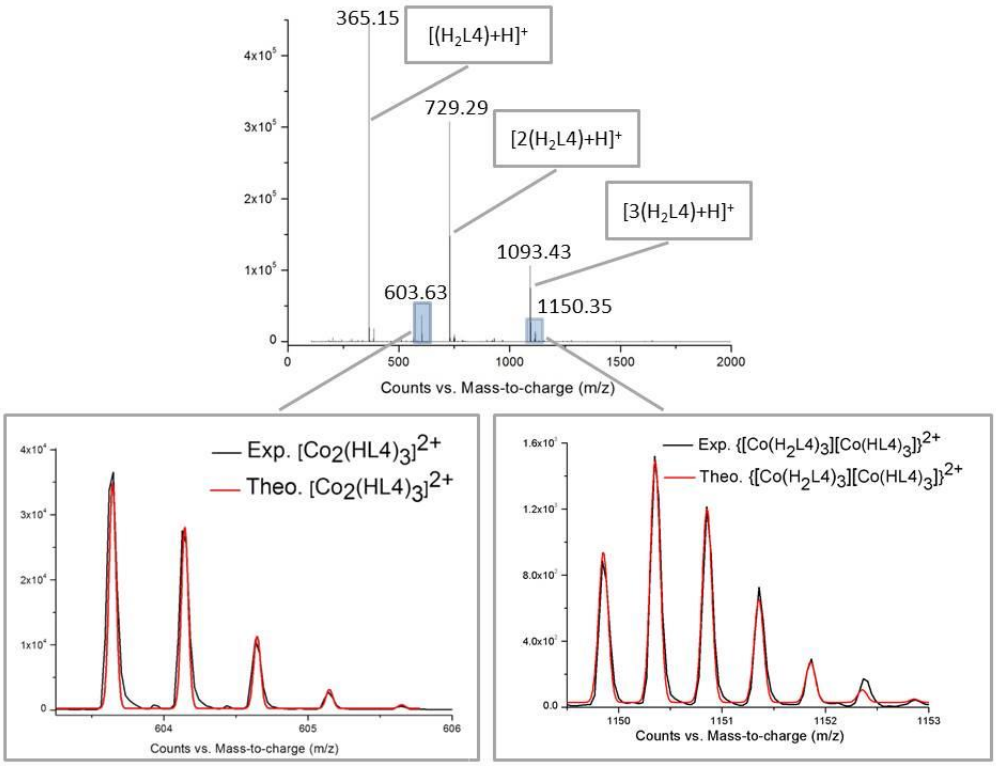

Figure 2.9: Mass spectrum of **iii** in CH_3CN (top) with peaks correspond to free ligand is assigned. Focusing on two peaks (bottom) and the match of theoretical and experimental isotopic distribution of dinuclear helicate $[Co_2(HL4)_3Cl]^{2+}$ (left) and dimerized helicate $\{[Co(H_2L4)_3][Co(HL4)_3]\}^{2+}$ (right) (see text for details).

Another metal assembly is also observed in the ESI-MS spectrogram corresponding to a dimerized helical structure. This assembly consists of two mononuclear triple stranded $[Co(H_2L4)_3]$ helicates forming a dimer through hydrogen bonds. Indeed, such assemblies were isolated in solid state for Fe(II) ions (see Chapter 4). Thus, a Fragment of this assembly at m/z = 1150.35 was observed which corresponds to $\{[Co(H_2L4)_3][Co(HL4)_3]\}^{2+}$. In this ion, three N-H units have been deprotonated and one cobalt ion has +3 charge. The Cl^- encapsulated dimerized helicate is not observed in contrast to the Fe(II) analogous compound (chapter 3).

The mass spectrogram of **iv** shows a prominent peak representing a dinuclear species $[Ni_2(HL4)_2]^{2+}$ at m/z = 421.07. Only two ligand molecules are present in this assembly, which could correspond to a double-stranded helicate or mesocate. The isotopic distribution of this peak is consistent with the theoretical one as shown in Figure 2.10. A very weak peak was also detected at m/z = 439.11, which corresponds to $\{[Ni_2(HL4)(L4)]Cl\}^{2+}$ (not shown in Figure 2.10). The nickel ion is here oxidized to

Ni(III) and the assembly could correspond to the Cl^- encapsulated double-stranded helicate. This assembly is different to the one observed in solid state, which is a triple stranded helicate.

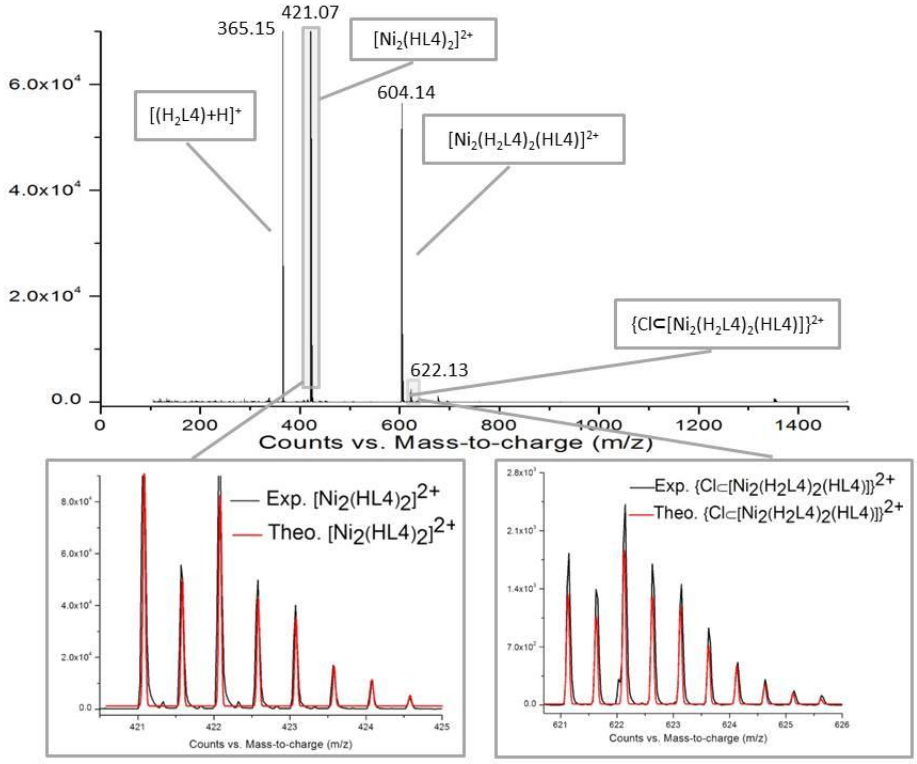

Figure 2.10: Mass spectrum of **iv** in CH_3CN (top) with peaks correspond to free ligand is assigned. Focusing on two peaks (bottom) and the match of theoretical and experimental isotopic distribution of dinuclear double-stranded helicate $[Ni_2(HL4)_2]^{2+}$ (left) and triple-stranded helicate $\{Cl\subset[Ni_2(H_2L4)_2(HL4)]\}^{2+}$ (right) (see text for details).

Another intense peak is observed at m/z = 604.14 and corresponds to the free-of-ion triple stranded helicate $[Ni_2(H_2L4)_2(HL4)]^{2+}$. The Cl^- encapsulated helicate $\{Cl\subset[Ni_2(H_2L4)_2(HL4)]\}^{2+}$ was also observed as a low intense peak at m/z = 622.13. The isotopic distribution of this peak is also consistent with the theoretical one as shown in Figure 2.10. Both triple and double stranded $[Ni]_2$ helicates seem stable in solution since their peaks have high intensity, while no other assemblies are observed. In contrast to metal helicates with Fe(II) and Co(II), no peaks corresponding to the dimerized mononuclear helicate (*i.e.* $\{[Ni(H_2L4)_3]_2\}^{4+}$) were detected.

2.4 Bigger Helical Cavity for Bigger Anions

The bis-pyrazolylpyridine moieties in H_2L4 show the ability to form triple-stranded binuclear helicates which encapsulated halide ions. However, the nature of the rigid phenyl spacer limits the ability of the assemblies to encapsulate bigger guests. Therefore, changing the phenyl spacer in H_2L4 to a larger and a more flexible one is the way to increase the volume of the cavity and thus increase the ability of the metal assembly to encapsulate bigger guests.

This goal was achieved by preparing a new bis-pyrazolylpyridine ligand (H_2L6) where the spacer between both pyrazolylpyridine parts is a 1,1'-biphenyl group (Figure 2.12). The ditopic nature of H_2L6, arising from two chelating sites, gives again the possibility to link two metal ions to yield stable dinuclear helicates. The 1,1'-biphenyl spacer group is a good candidate to form bigger cavities since it has the ability to twist around the C-C bond attaching the two phenyl rings in addition to the ability of twisting around the C-C bond linking the biphenyl group with the pyrazole rings.

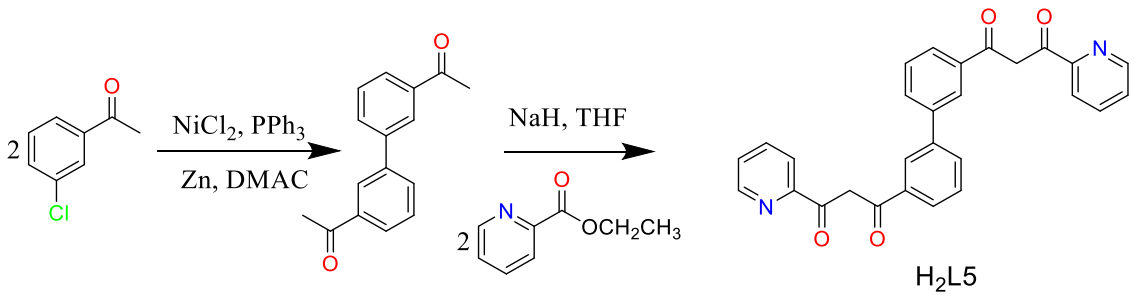

Figure 2.11: Synthesis of diketone precursor H_2L5 {3,3'-([1,1'-biphenyl]-3,3'-diyl)bis(1-(pyridin-2-yl)propane-1,3-dione)}.

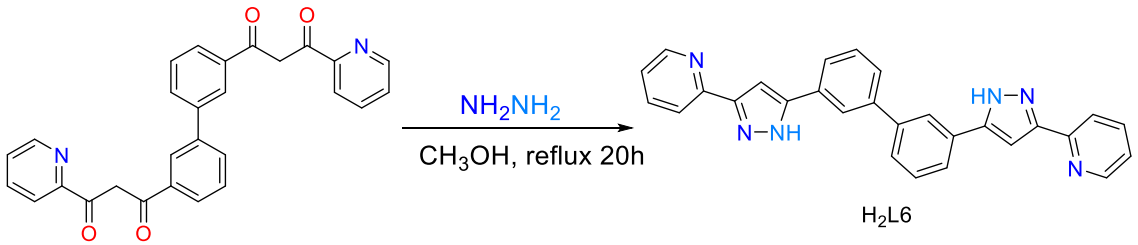

Figure 2.12: Synthesis of the ligand H_2L6 {3,3'-bis(3-(pyridin-2-yl)-1H-pyrazol-5-yl)biphenyl}

In order to synthesize the H_2L6, the diketone precursor, H_2L5, was synthesized by the Claisen condensation reaction of 3,3'-diacetylbiphenyl with ethyl 2-picolinate in THF, using NaH as a base (Figure 2.11). 3,3'-diacetylbiphenyl was synthesized by the nickel-

catalyzed coupling reaction according to a literature procedure.[38] The ^{1}H NMR of H_2L5 shows a broad peak at 16.43 ppm corresponding to OH enol group. The relative intensity of this peak with the aromatic C-H peaks indicates that mostly the enol form of the ligand is present in chloroform. The ligand H_2L6 was then prepared via the ring closure reaction of H_2L5 with hydrazine in methanol (Figure 2.12). After refluxing for 20 h, H_2L6 was collected as a white solid in around 50 % yield. The ligand was characterized by ^{1}H NMR, mass spectrometry and elemental analysis (see experimental section).

Using this ligand, [Fe(II)$_2$] triple-stranded helicates that encapsulate M(oxalate)$_3$ complexes as guest are formed (chapter 5) which confirms the flexibility of such ligand to form big cavities. Moreover, a ClO_4⊂[Fe(II)$_2$] triple stranded helicate was also synthesized, which exhibits gradual SCO. This compound will be described in the following section.

2.4.1 Synthesis and Crystal Structure of ClO_4⊂[$Fe_2(H_2L6)_3$](ClO_4)$_3$·16CH_3CN (v)

Compound **v** was prepared by treating the reaction mixture of Fe(CF_3SO_3)$_2$·6H_2O and H_2L6 in methanol with excess of NBu_4ClO_4, which yielded a heavy precipitate. The solid was collected and then dissolved in acetonitrile, and the resulting solution was vapor diffused with ether at 5 °C yielding red crystals after a few days.

Compound **v** crystallizes in the triclinic space group *P-1* (*Z*=2). Crystal data and selected structural parameters at 100 K are shown in and Tables 2.4 and 2.5. The asymmetric unit consists of a cationic encapsulating helicate {ClO4⊂[$Fe_2(H_2L6)_3$]}$^{3+}$, three ClO_4^- external anions and four CH_3CN solvent molecules. Moreover, twelve additional diffused CH_3CN molecules were determined using PLATON SQUEEZE function.[39] Three H_2L6 ligands wrap around the principal axis formed by the two Fe(II) centers in a pseudo-S shape to form the triple-stranded helicate (Figure 2.13). Both Fe(II) centers exhibit a pseudo-octahedral coordination environment arising from three pyrazolylpyridine chelating groups. As the ligand has C2-symmetry, the resulting helicate has D_3-symmetry. It has a C_3 axis coincident with the Fe···Fe helical axis, and three C_2 axes, which are perpendicular to the helical axis. Both metal ions in each discrete helicate have the same chirality. Each complex is thus either *ΔΔ* or *ΛΛ*, leading

to a racemic mixture of two enantiomers. The intrahelical Fe1···Fe2 distance is 11.018 Å.

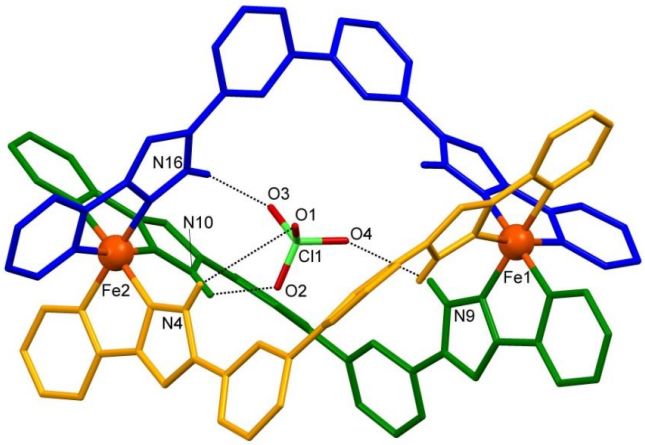

Figure 2.13: Molecular representation of $\{ClO_4 \subset [Fe_2(H_2L6)_3]\}^{3+}$ cation in **v** showing the hydrogen bonding between the NH groups and the oxygen atoms of the encapsulated perchlorate . Three ClO_4^- ions and acetonitrile solvent molecules are omitted for clarity. Only the hydrogen atoms on the pyrazole nitrogen atoms are shown. Only metals and heteroatoms involved in hydrogen bonding are labeled.

The helicate encapsulates one ClO_4^- anion that locates close to Fe2 center [Fe2···Cl1 = 4.983 and Fe1···Cl1 = 6.075 Å] as a result of the stronger hydrogen bonding with N-H groups in this side of the helicate (Figure 2.13 and Table 2.5). The flexibility of the biphenyl spacer produces a larger cavity able of encapsulating a bigger anion. To obtain the helical shape, the biphenyl group exhibit *cis* like conformation, arising from twisting around the central C-C bond. The three ligands exhibit similar torsion angles between the two phenyl rings in the biphenyl group (average angle of 43.93°) as a way to offer the suitable symmetry around both Fe(II) centers. Additional twisting is observed between the pyrazole and the phenyl groups, which falls in the range 9.71-21.33°. This twist also helps to adopt the helical structure by the ligands. Interestingly, the pyrazolyl-pyridine moieties are almost within the same plane, with twisting angles less than 6°.

The Fe-N_{avg} distances are 1.960 Å and 1.975 Å for (Fe1-N) and (Fe2-N), respectively. This indicates a low spin configuration for both Fe(II) centers at 100 K in agreement with bulk magnetic studies (see below). Moreover, the distortion parameters Σ and Θ (Table 2.5) for both iron centers are similar to that seen for LS Fe(II) centers in the other helicates (chapter 3). The contiguous helicates, of opposite chirality, in the

unit cell are interacting via $\pi-\pi$ interactions between the biphenyl groups with centroid to centroid distance of 4.925 Å (Figure 2.14)

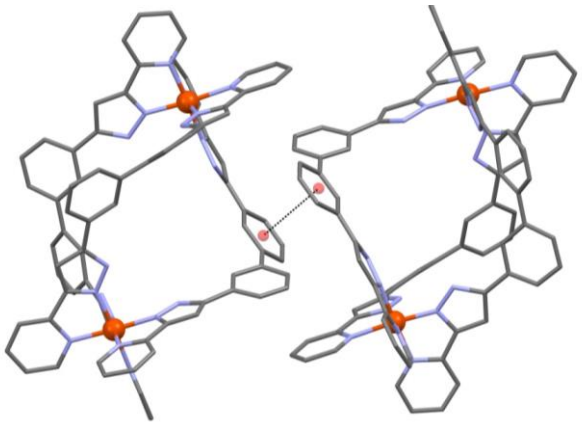

Figure 2.14: The packing of the contiguous helicates in **v** which results from $\pi-\pi$ (4.925 Å) interactions between biphenyl groups of the neighbor helicates.

Table 2.4: Crystallographic data for **v**

Compound	**v**
Formula	$C_{84}\,H_{60}\,Fe_2\,N_{18}$, 4(Cl O_4), 16($C_2\,H_3\,N$)
Mr	2487.84
wavelength	0.71073
T (K)	100 K
Crystal system	Triclinic
Space group	*P-1*
Z	2
a [Å]	18.685(2)
b [Å]	19.364(2)
c [Å]	19.401(2)
α [º]	68.021(6)
β [º]	88.515(7)
γ [º]	67.719(6)
V [Å^3]	5968.1(11)
ρ_{calc} (gcm^{-3})	1.384
μ(mm-1)	0.491
Independent reflections	7171
Restraints / parameters	1429/ 1204
Goodness of fit on F^2	1.036
Final R_1/wR_2 [$I>2\sigma(I)$]	0.1165/ 0.2911
Final R_1/wR_2 [all data]	0.1574/ 0.3269
Largest diff. peak and hole (eÅ^3)	1.406/ -1.155

Table 2.5: Selected interatomic distances [Å] and selected structural factors found in **v**

Fe1-N1	2.01(2)	Fe2-N5	1.92(1)
Fe1-N2	1.93(1)	Fe2-N6	2.00(2)
Fe1-N7	1.96(1)	Fe2-N11	1.97(1)
Fe1-N8	1.96(2)	Fe2-N12	2.01(1)
Fe1-N13	2.00(1)	Fe2-N17	1.95(2)
Fe1-N14	1.96(1)	Fe2-N18	1.98(1)
Fe1⋯Fe2	11.018(4)	Fe1⋯Cl1	6.075(9)
Fe2⋯Cl1	4.983(9)	N16-H⋯O3	2.14
N4-H⋯O1	3.19	N9-H⋯O4	2.69
N10-H⋯O2	2.44		
$(Fe\text{-}N)_{avg}$[a]	1.960/1.975	Σ(°)[a]	60.6/66.8
Θ(°)[a]	194.0/207.0	V_{oct}(Å^3)[a]	10.023/10.019

a: In Fe1/Fe2 form

2.4.2 Magnetic Properties of $ClO_4 \subset [Fe_2(H_2L6)_3](ClO_4)_3 \cdot 16CH_3CN$ (v)

Magnetic susceptibility measurements of compound **v** were carried out on a polycrystalline sample in the temperature range 2-350 K, under a constant magnetic field of 0.5 T. Plots of $\chi_m T$ vs. T in the heating and the cooling mode are shown in Figure 2.15. Upon heating, the $\chi_m T$ value below 200 K remains constant at around 0.45 $cm^3mol^{-1}K$ indicating a LS state states of the two Fe(II) centers with less than 6 % of residual HS Fe(II) centers. This agrees with the crystal structure at 100 K which showed both Fe(II) centers to be in the LS state. A gradual SCO behavior was observed starting from 200 K up to 350 K, with a maximum $\chi_m T$ value of 7.21 $cm^3mol^{-1}K$. This corresponds to a LS→HS SCO of both iron Fe(II) centers.

There is no clear plateau at high temperatures which indicates that the distribution of HS/LS centers is statistical throughout the lattice at all temperatures. The SCO is centered at around 320 K. In cooling, a significant difference in the magnetic behavior was observed with respect to the warming mode. Below 350 K, the $\chi_m T$ decreased in a more gradual fashion down to 80 K with $\chi_m T$ = 0.75 $cm^3mol^{-1}K$. The SCO process in the cooling mode occurs over a larger temperature range than the heating mode. The loss of some solvent molecules from the lattice at high temperatures is the most likely reason of such change in magnetic response between the heating and the cooling sweeps.

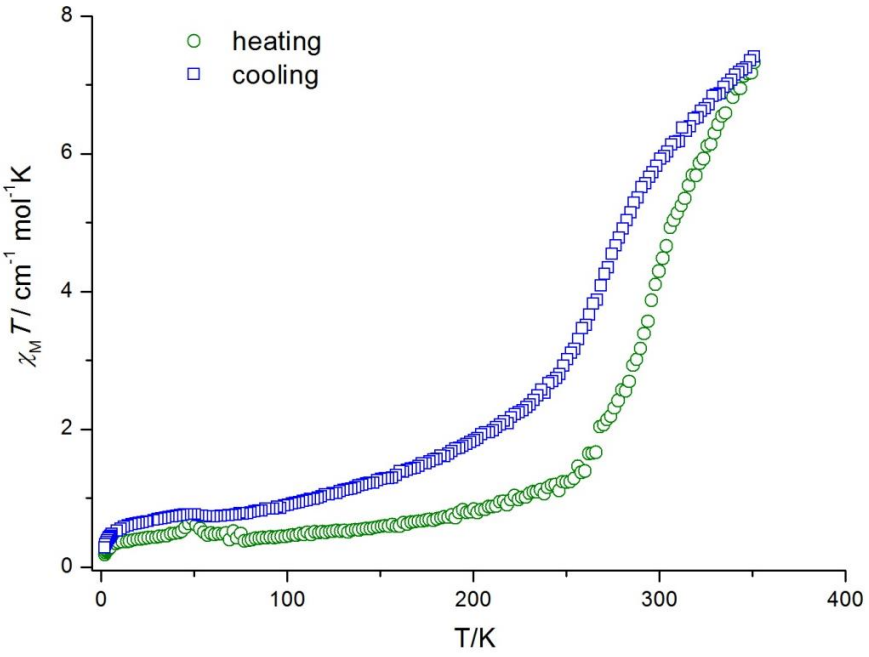

Figure 2.15: Variable temperatures magnetic susceptibility measurements of **v** measured at 0.5 T dc magnetic field in the heating and the cooling sweeps.

2.5 Conclusions

Two novel bis-pyrazolyl-pyridine ligands were synthesized from the ring closure reaction of their corresponding *β*–diketone precursors. The ligands were used to prepare dinuclear triple stranded helicates with cobalt, nickel or iron metal divalent ions. The helicates encapsulate chloride anion in the case of the ligand with a phenyl as spacer between both pyrazolyl-pyridine moieties. The cavity formed by this ligand is small to encapsulate bigger anions. Changing the spacer to biphenyl groups yielded helicates with a bigger cavity that could then encapsulate a perchlorate anion inside their cavity. This encapsulation of anions happens thanks to the hydrogen bonding interactions with the N-H groups, which are directed towards the inside of the helical cavity. Moreover, the dinuclear Fe(II) helicate exhibit SCO at both metal centers from the LS to the HS states. The following chapters will discuss the use of these ligands to prepare novel host-guest Fe(II) helicates, which encapsulate halides anions or metal complexes and exhibit novel SCO behavior.

2.6 Experimental

1-(2-hydroxyphenyl)-3-(3-(3-oxo-3-phenylpropanoyl)phenyl)propane-1,3-dione H_2L1. See appendix I

1,3-*bis*-(3-oxo-3-(2-methoxyphenyl)-propionyl)-pyridine H_2L2. See appendix I

1,3-*bis*-(1-oxo-3-(pyridine-2-yl)-propionyl)-benzene, H_2L3. To a suspension of 60% NaH oil dispersion (2g, 50 mmol) in 150 ml THF was added 1,3-diacetylbenzene (2g, 12.3 mmol) and the mixture was stirred for 15 minutes. Then 2-ethylpicolinate (3.4 ml, 24.7 mmol) in 50 ml THF was added dropwise, and the mixture brought and left to reflux overnight. A green-mustard suspension was formed after that, which was quenched with 5 ml EtOH and the resulting solid was then collected by filtration. The solid was suspended in 150 ml H_2O, the pH was adjusted to 2-3 using 12% HCl and the mixture was left 30 minutes under stirring. The yellow solid was collected by filtration, washed with water and dried under vacuum. The yield was 3.4 g (73.8 %).^{1}H NMR in $CDCl_3$, δ (ppm): 7.43 (*m*, 2H); 7.56 (*m*, 2H); 7.66 (*s*, 2H); 7.86 (*t*, 2H); 8.16 (*d*, 2H); 8.21 (*dd*, 2H); 8.69 (*m*, 2H); 16.45 (broad *s*, 2H). m/z = 373.12 $(M+H)^+$.

1,3-*bis*-(1-(pyridine-2-yl)-pyrazol-3-yl)-benzene, H_2L4. Solid H_2L3 (1.5 g, 4 mmol) was suspended in CH_3OH (70 ml) and excess hydrazine (64% in H_2O, 2.6 ml, 34.3 mmol) was added to the mixture dropwise. The mixture turned with time to clear orange solution to yield a white solid through reflux for 20h. The mixture is cooled to room temperature and the solid was collected by filtration, washed with CH_3OH and water and dried under vacuum. The yield was 0.70 g (48 %). ^{1}H NMR in DMSO, δ (ppm):7.32 (*t*, 2H); 7.46 (*s*, 2H); 7.54 (*t*, 1H); 7.90 (*m*, 6H); 8.40 (*s*, 1H); 8.63 (*s*, 2H); 13.52 (very broad, NH groups).*Anal. Calc.* (Found) for $\mathbf{H_2L4}\cdot 0.5H_2O$: C, 70.76 (70.39); H, 4.59 (4.37); N, 22.51 (22.48). m/z = 365.17 $(M+H)^+$.

3,3'-diacetylbiphenyl. The compound was prepared according to the procedure described in the literature.[38]

3,3'-bis(1-(pyridin-2-yl)propane-1,3-dione)biphenyl, H_2L5. To a suspension of 60% NaH oil dispersion (1.6 g, 40 mmol) in 100 ml THF was added 3,3'-diacetylbiphenyl (2g, 8.4 mmol) and the mixture was stirred for 15 minutes. Then 2-ethylpicolinate (2.3 ml, 16.8mmol) in 50 ml THF was added dropwise, and the mixture brought and left to reflux overnight. A green-mustard suspension was formed after that, which was

quenched with 5 ml EtOH and the resulting solid was then collected by filtration. The solid was suspended in 150 ml H_2O, the pH was adjusted to 2-3 using 12% HCl and the mixture was left 30 minutes under stirring. The yellow solid was collected by filtration, washed with water and dried under vacuum. The yield was 2.9 g (77.1 %).^{1}H NMR in $CDCl_3$, δ (ppm): 7.41(*ddd*, 2H); 7.54 (*m*, 2H); 7.66 (*s*, 2H); 7.86 (*m*, 4H); 8.02 (*td*, 2H); 8.14 (*dd*, 2H); 8.26 (*t*, 2H); 8.68 (*ddd*, 2H), 16.43 (broad *s*, 2H). *Anal. Calc.* (Found) for **H_2L5** (+1.7H_2O, 0.25C_4H_8O): C, 70.35 (70.12); H, 4.76 (4.38); N, 5.66 (5.27). m/z = 449.15 $(M+H)^+$.

3,3'-bis(3-(pyridin-2-yl)-1H-pyrazol-5-yl)biphenyl, **H_2L6.** The ligand H_2L5 (1.5 g, 3.3mmol) was suspended in CH_3OH (70 ml) and excess hydrazine (64% in H_2O, 2.6 ml, 34.3 mmol) was added to the mixture dropwise. The mixture turned with time to clear orange solution to yield a white solid through reflux for 20h. The mixture is cooled to room temperature and the solid was collected by filtration, washed with CH_3OH and water and dried under vacuum. The yield was 0.74 mg (50 %). ^{1}H NMR in $CDCl_3$, δ (ppm):7.06 (*s*, 2H); 7.18 (*m*, 2H); 7.46 (*t*, 2H); 7.60 (*d*, 2H); 7.74 (*m*, 4H); 7.80 (*d*, 2H); 8.12 (*s*, 2H); 8.65 (*d*, 2H).*Anal. Calc.* (Found) for **H_2L6** (+0.45 H_2O): C, 74.97 (75.00); H, 4.70 (4.62); N, 18.73 (18.85). m/z = 441.19 $(M+H)^+$.

[$Fe_2(H_2L1)_3$] (i). A suspension of H_2L1 (10 mg, 0.026 mmol) and triehtylamine (7.2 μL, 0.052 mmol) in CH_2Cl_2 was stirred for 30 min. Then $FeCl_3.6H_2O$ (4.7 mg, 1.74 mmole) in 2 ml CH_2Cl_2 was added dropwise. The resulted solution was refluxed for 1 hour. After cooling down the solution was filtered off and layered with toluene. Crystals suitable for single crystal x-ray diffraction was obtained after two weeks. The yield was 2.5 mg (22.7 %).

[K⊂$Fe_2(H_2L2)_3$]($FeCl_4$) (ii). A suspension of H_2L2 (40 mg, 0.092 mmol) in THF (10 mL) was added dropwise to a THF solution (10 mL) of $FeCl_3.6H_2O$ (35.1 mg, 0.12 mmol) and K_2CO_3 (12.7 mg 0.092 mmol). A deep red solution formed which was stirred for 45 minutes, filtered off and layered with toluene. Red crystals suitable for single crystal x-ray diffraction were formed after a few days. The yield was 11.5 mg (23.0%).

Cl⊂[$Co_2(H_2L)_3$]Cl(PF_6)$_2$·4CH_3OH.0.25$C_4H_{10}O$ (iii). A suspension of H_2L (25 mg, 0.069 mmol) in methanol (10 mL) was added dropwise to a methanolic solution (5 mL) of $CoCl_2.6H_2O$ (10.9 mg, 0.046 mmol). An orange solution formed, which was stirred

for 45 minutes, filtered and the filtrate treated with a methanolic (2 mL) solution of NBu_4PF_6 (14 mg, 0.036 mmol) and stirred for ten minutes. The resulting solution was layered with ether, which yielded red crystals after a few days. The yield was 19 mg (48%). *Anal. Calc.* (Found) for **iii (**+1.65H_2O): C, 48.91 (48.78); H, 4.18 (4.02); N, 14.27 (14.42).

Cl⊂[$Ni_2(H_2L)_3$]Cl(PF_6)$_2$·5CH_3OH (iv). A suspension of H_2L (25 mg, 0.069 mmol) in methanol (10 mL) was added dropwise to a methanolic solution (5 mL) of $NiCl_2.6H_2O$ (10.8 mg, 0.046 mmol). A pink solution formed, which was stirred for 45 minutes, filtered and the filtrate treated with a methanolic (2 mL) solution of NBu_4PF_6 (14 mg, 0.036 mmol) and stirred for ten minutes. The resulting solution was layered with ether, which yielded red crystals after a few days. The yield was 8 mg (20%). *Anal. Calc.* (Found) for **iv** (+4.95 H_2O): C, 46.45 (46.83); H, 3.91 (4.31); N, 13.78 (13.85).

ClO_4⊂[$Fe_2(H_2L6)_3$](ClO_4)$_3$·16CH_3CN (v). A suspension of H_2L6 (25 mg, 0.057 mmol) in methanol (10 mL) was added dropwise to a methanolic solution (5 mL) of $Fe(CF_3SO_3)_2.6H_2O$ (17.4 mg, 0.038mmol). A red solution formed which was stirred for 45 minutes and then filtered off. The resulted solution was treated with methanolic solution (5ml) of 10-fold excess of NBu_4ClO_4 and stirred for 10 minutes which yielded a heavy precipitate. The solid was collected and then dissolved in acetonitrile. The red solution was vapor diffused with ether at 5 C̊ which yielded red crystals after few days. The yield was 10.2 mg (21.6 %). *Anal. Calc.* (Found) for **v** (-14 CH_3CN, + 6H_2O**)**: C, 52.29 (51.98); H, 3.89 (3.61); N, 13.86 (13.49).

2.7 References

1 E. C. Sañudo, J. S. Uber, A. Pons Balagué, O. Roubeau and G. Aromí, *Inorg. Chem.*, 2012, **51**, 8441–8446.

2 D. Aguilá, L. A. Barrios, F. Luis, A. Repollés, O. Roubeau, S. J. Teat and G. Aromí, *Inorg. Chem.*, 2010, **49**, 6784–6786.

3 D. Aguilà, L. a Barrios, O. Roubeau, S. J. Teat and G. Aromí, *Chem. Commun. (Camb).*, 2011, **47**, 707–9.

4 L. A. Barrios, D. Aguilá, O. Roubeau, P. Gamez, J. Ribas-Ariño, S. J. Teat and G. Aromí, *Chem. - A Eur. J.*, 2009, **15**, 11235–11243.

5 L. A. Barrios, A. D. Aguilà, A. O. Roubeau and B. K. S. Murray, *Aust. J. Chem.*, 2009, **62**, 1130–1136.

6 G. Aromi, P. Gamez and J. Reedijk, *Coord. Chem. Rev.*, 2008, **252**, 964–989.

7 D. Aguila, L. A. Barrios, V. Velasco, O. Roubeau, A. Repolles, P. J. Alonso, J. Sese, S. J. Teat, F. Luis and G. Aromi, *J. Am. Chem. Soc.*, 2014, **136**, 14215–14222.

8 G. Aromí, D. Aguilà, P. Gamez, F. Luis and O. Roubeau, *Chem. Soc. Rev.*, 2012, **41**, 537.

9 F. Luis, A. Repollés, M. J. Martínez-Pérez, D. Aguilá, O. Roubeau, D. Zueco, P. J. Alonso, M. Evangelisti, A. Camón, J. Sesé, L. A. Barrios and G. Aromí, *Phys. Rev. Lett.*, 2011, **107**, 1–4.

10 O. V. Dolomanov, L. J. Bourhis, R. J. Gildea, J. A. K. Howard and H. Puschmann, *J. Appl. Crystallogr.*, 2009, **42**, 339–341.

11 R. D. Shannon, *Acta Crystallogr. Sect. A*, 1976, **32**, 751–767.

12 L. A. Barrios, E. Peyrecave-Lleixá, G. A. Craig, O. Roubeau, S. J. Teat and G. Aromí, *Eur. J. Inorg. Chem.*, 2014, **2014**, 6013–6021.

13 J. S. Costa, S. Rodríguez-Jimenez, G. A. Craig, B. Barth, C. M. Beavers, S. J. Teat and G. Aromí, *J. Am. Chem. Soc.*, 2014, **136**, 3869–3874.

14 G. A. Craig, O. Roubeau and G. Aromí, *Coord. Chem. Rev.*, 2014, **269**, 13–31.

15 G. a Craig, J. S. Costa, O. Roubeau, S. J. Teat, H. J. Shepherd, M. Lopes, G. Molnár, A. Bousseksou and G. Aromí, *Dalton Trans.*, 2014, **43**, 729–37.

16 G. A. Craig, J. S. Costa, O. Roubeau, S. J. Teat and G. Aromí, *Eur. J. Inorg. Chem.*, 2013, 745–752.

17 G. A. Craig, J. S. Costa, O. Roubeau, S. J. Teat and G. Aromí, *Chem. - A Eur. J.*, 2012, **18**, 11703–11715.

18 G. A. Craig, J. Sánchez costa, O. Roubeau, S. J. Teat and G. Aromí, *Chem. - A Eur. J.*, 2011, **17**, 3120–3127.

19 G. A. Craig, L. A. Barrios, J. S. Costa, O. Roubeau, E. Ruiz, S. J. Teat, C. C. Wilson, L. Thomas and G. Aromí, *Dalt. Trans.*, 2010, **39**, 4874.

20 M. A. Halcrow, *Spin-crossover materials: properties and applications*, John Wiley & Sons, 2013.

21 P. Gütlich and H. A. Goodwin, *Spin crossover in transition metal compounds I*, Springer Science & Business Media, 2004.

22 D. L. Caulder and K. N. Raymond, *J. Chem. Soc. Dalt. Trans.*, 1999, 1185–1200.

23 F. Lloret, M. Julve, J. Cano, R. Ruiz-García and E. Pardo, *Inorganica Chim. Acta*, 2008, **361**, 3432–3445.

24 O. Kahn, *Molecular Magnetism*, VCH Publishers, Inc., New York, 1993.

25 J. Vallejo, I. Castro, R. Ruiz-Garcia, J. Cano, M. Julve, F. Lloret, G. De Munno, W. Wernsdorfer and E. Pardo, *J. Am. Chem. Soc.*, 2012, **134**, 15704–15707.

26 E. Colacio, J. Ruiz, E. Ruiz, E. Cremades, J. Krzystek, S. Carretta, J. Cano, T. Guidi, W. Wernsdorfer and E. K. Brechin, *Angew. Chemie Int. Ed.*, 2013, **52**, 9130–9134.

27 H. Sakiyama, T. Suzuki, K. Ono, R. Ito, Y. Watanabe, M. Yamasaki and M. Mikuriya, *Inorganica Chim. Acta*, 2005, **358**, 1897–1903.

28 H. Sakiyama, R. Ito, H. Kumagai, K. Inoue, M. Sakamoto, Y. Nishida and M. Yamasaki, *Eur. J. Inorg. Chem.*, 2001, 2027–2032.

29 J. M. Herrera, A. Bleuzen, Y. Dromze, M. Julve, F. Lloret, M. Verdaguer and M. Curie, *Society*, 2003, **42**, 7052–7059.

30 V. Mishra, F. Lloret and R. Mukherjee, *Inorganica Chim. Acta*, 2006, **359**, 4053–4062.

31 S. Konar, E. Zangrando, M. G. B. Drew and N. Ray, 2004.

32 R. Herchel, L. Váhovská, I. Potocnak and Z. Trávnícek, *Inorg. Chem.*, 2014, **53**, 5896–5898.

33 V. Chandrasekhar, A. Dey, A. J. Mota and E. Colacio, *Inorg. Chem.*, 2013, **52**, 4554–4561.

34 M. A. Halcrow, *Chem. Soc. Rev.*, 2011, **40**, 4119–4142.

35 S. Alvarez, D. Avnir, M. Llunell and M. Pinsky, *New J. Chem.*, 2002, **26**, 996–1009.

36 N. F. Chilton, R. P. Anderson, L. D. Turner, A. Soncini and K. S. Murray, *J. Comput. Chem.*, 2013, **34**, 1164–75.

37 R. Boca, *Coord. Chem. Rev.*, 2004, **248**, 757–815.

38 H.-F. Li, P.-F. Yan, P. Chen, Y. Wang, H. Xu and G.-M. Li, *Dalton Trans.*, 2012, **41**, 900–7.

39 A. L. Spek, *Acta Crystallogr. Sect. C, Struct. Chem.*, 2015, **71**, 9–18.